Journal of Electronic Materials (2026) 55:4528–4538
https://doi.org/10.1007/s11664-026-12782-5

ORIGINAL RESEARCH ARTICLE

Ab Initio Modeling of Mg*X*Ir$_2$ (*X* = Al, Ga, In, Si): A Multifaceted Study on Physical Properties

Songül Oğlakçi[1] · Cevat Aksu[1] · Murat Çanli[2] · Nihat Arikan[1]

Received: 21 October 2025 / Accepted: 28 February 2026 / Published online: 14 March 2026

Abstract

We present a comprehensive *ab initio* investigation of the structural, electronic, mechanical, thermodynamic, and vibrational properties of Mg*X*Ir$_2$ (*X* = Al, Ga, In, Si) full-Heusler compounds using density functional theory (DFT). Structural optimization reveals that all four compounds stabilize in the cubic Fm3m phase, with lattice parameters showing a monotonic increase from *X* = Si to In. Electronic band structure calculations demonstrate metallic behavior, characterized by Ir-*d* orbital dominance near the Fermi level. Mechanical properties, including elastic constants (C_{11}, C_{12}, C_{44}), confirm thermodynamic stability and ductile behavior, with MgSiIr$_2$ exhibiting the highest bulk modulus (218 GPa). Phonon dispersion spectra show no imaginary frequencies, verifying dynamic stability across all compositions. Thermodynamic analysis via quasi-harmonic approximation predicts Debye temperatures ranging from 420 K (MgInIr$_2$) to 580 K (MgSiIr$_2$), correlating with bond stiffness trends. Vibrational modes indicate distinct optical phonon splitting is the highest in MgSiIr$_2$ owing to mass contrast. The Grüneisen parameters suggest anharmonic effects are most pronounced in MgInIr$_2$. Comparative analysis highlights MgSiIr$_2$ as the most promising candidate for high-temperature applications, balancing mechanical strength and thermal stability. This work provides foundational insights into experimental synthesis and targeted applications in catalysis or spintronics. Given magnesium's osteogenic properties, these alloys also hold significant potential in regenerative medicine, particularly for repairing osseous defects triggered by degenerative disorders or bone cancer.

Keywords *Ab initio* · DFT · Heusler compounds · physical properties

Introduction

Research in materials science has prioritized Heusler materials because their property tunability permits the engineering of systems with elevated Curie temperatures and optimized electronic configurations.[1–9] Intermetallic compounds have many different appealing combinations of Heusler alloys for topological insulators[5,10] and thermoelectric materials.[11-13] Besides, they can be employed as spin gapless semiconductors, materials with shape memory, and other types of thermoelectric materials.[14–17] The stoichiometric configurations of Heusler group materials are XYZ, X_2YZ, and XYMZ. In these configurations, X, Y, and M are usually transition metals and Z is the most important group that provides electronic and structural endurance. Full-Heusler compounds have a cubic crystal structure with a stoichiometry of 2:1:1 (X_2YZ). X_2YZ Heusler compounds can be characterized into two diverse types: (1) the cubic $L2_1$ structure with space group Fm3m having the $AlCu_2Mn$ prototype, and (2) the $CuHg_2Ti$ type structure with space group F43m.[18]

Magnesium (Mg) has properties similar to human bone in terms of biocompatibility, mechanical strength, and biodegradation, and better properties are achieved in studies conducted with the aim of forming Mg-based compounds with other metals.[19] Among those compounds, many researchers are also interested in Ir-based Heusler alloys because of their potential half-metallic properties and structural stability, as well as their significant applications in next generation computation accelerators, data storage systems, tunneling magnetic resonance (TMR), and giant magnetoresistance (GMR).[20-22] Studies on Heusler alloys related to Ir-based compounds generally consider the $L2_1$ structure.[23,24] The scientific understanding of Ir-based Heusler alloys is currently constrained by a scarcity of experimental

✉ Murat Çanli
murat.canli@ahievran.edu.tr

[1] Osmaniye Korkut Ata University, Osmaniye, Turkey

[2] Kirsehir Ahi Evran University, Kirsehir, Turkey

and theoretical studies. The magnetic properties and crystal structure of Ir_2MnGa and Ir_2MnAl alloys were determined experimentally in early studies by Masumoto et al.[25] Likewise, density function theory (DFT) computations were used to study the electronic structure, magnetic, half-metallic, elastic, and thermodynamic characteristics of Ir_2MnAl and Ir_2MnGa complete Heusler alloys.[26] Furthermore, Krishnaveni[27] theoretically investigated the full-Heusler Ir_2VX (*X* = Ga and Ge) alloys. In addition, Ir_2MnAl were theoretically studied in terms of the lattice parameter, magnetic properties and electronic structure.[28,29] Forozani et al.[30] conducted an *ab initio* calculation to evaluate the structural, electronic, magnetic, and phonon characteristics of the full-Heusler Ir_2CrSi and Ir_2CrGe alloys. In another study, Forozani investigated Ir_2ScZ full-Heusler alloys (*Z* = Si, Ge, Sn) to find out their structural, electronic, magnetic, and optical properties[31] using density functional theory (DFT). The different physical properties of full-Heusler Ir_2MnSi have been investigated by Özdemir et al.[32] within the framework of the *ab initio* method. Gupta et al.[33] studied the mechanical and thermodynamic properties of newly proposed Ir_2V (In, Sn) Heusler alloys and suggested that these alloys may be suitable for high-temperature thermoelectric applications owing to their half metallic properties. The electronic and thermoelectric (TE) properties were also investigated using DFT by Balakrishnan et al. on Ir_2MnX (*X* = B, Al, Ga, In).[23] They revealed half-metallic behavior based on the alloys' finite magnetic moment and electronic characteristics, indicating their applicability for spintronic and TE device applications. A series of fully Heusler Ir_2YSi (*Y* = Ni, Co, Fe, Mn, Cr, Sc, V, and Ti) alloys in $L2_1$ (Cu_2MnAl) and Xa (Hg_2CuTi structure) phases were investigated by Prakash et al.[34] using density functional theory (DFT). They have proven the stability of these alloys in a cubic structure $L2_1$ and their ferromagnetic properties. An in-depth characterization of the full-Heusler $AlXIr_2$ (*X* = Co, Cr, Cu, Fe and Zn) alloys in terms of their mechanical and dynamic stability has been conducted by İyigör et al.[35] In a previous study,[36] the electronic band structure, thermodynamic, mechanical, and lattice dynamic properties of the Ir_2ScAl alloy were investigated using density functional theory (DFT). The computational evidence supports that the Ir_2ScAl alloy is both mechanically and dynamically stable in the $L2_1$ phase.

A systematic investigation of the physical characteristics of Full Heusler Mg*X*Ir$_2$ (*X* = Al, Ga, In, and Si) alloys has yet to be conducted, as far as we are aware. Thus, the structural, electronic, mechanic, thermodynamic, and vibrational characteristics of these materials are the focus of this investigation. These characteristics are appealing to the researchers for thermoelectric applications. The following is the paper's outline: the study's computational techniques are explained in Sect. "Method of Calculations," the material's structural, electrical, thermodynamic, and vibrational characteristics are examined in Sect. "Results," and closing thoughts are included in Sect. 4.

Method of Calculations

Employing DFT with a plane-wave pseudopotential approach, ground-state features were analyzed inside the Quantum-Espresso framework.[37] The generalized gradient approximation and Perdew, Burke and Ernzerhof were used to account for electronic exchange and correlation energy.[38] Planet wave cutoff energy and charge density cutoff were arranged at 50 Ry and 500 Ry, respectively, to achieve convergence. The integration in the first Brillouin zone was performed using the Monkhorst–Pack technique[39] with a **k**-mesh of 10 × 10 × 10. Density functional perturbation theory (DFPT) has been used to construct the full phonon spectra.[40, 41] The interatomic force constants were derived through Fourier interpolation of the dynamical matrices, employing a 4 × 4 × 4 q-mesh for sampling. The quasi-harmonic approximation (QHA) employed via ThermoPW includes full volume dependence. Thermal expansion was treated self-consistently by minimizing F(V, T) at each temperature. It is therefore not an isochoric treatment. Elastic and thermodynamic parameters could be extracted by using the energy-strain technique in the thermo-pw code. Mechanical characteristics were enlightened by the elastic constants. The ELATE code[42] was used to conduct mechanical properties analysis utilizing the elastic tensor components. The mechanical characteristics, such as bulk modulus (*B*), shear modulus (*G*), Young's modulus (*E*), Poisson's ratio (σ), and Pugh's ratio (*B*/*G*), were computed using the Voigt, Reuss, and Voigt–Reuss–Hill average approximations.[43]

Results

Mg*X*Ir$_2$ (*X* = Al, Ga, In and Si) alloys with a general formula of X_2YZ, as members of the full Heusler group,[44-47] crystallize in the $L2_1$ phase in the Fm3m space group, as seen in Fig. 1. The estimated equilibrium lattice constants of the compounds are provided in Table I. The results show strong accordance with the existing theoretical data.[44, 48] The formation enthalpy of Mg*X*Ir$_2$ (*X* = Al, Ga, In, and Si) compounds were computed as follows[45] to test thermodynamic stability and synthesizability.

$$\Delta E_f = E_{T_{(MgXIr_2)}} - \left(E_{Mg} + E_X + 2E_{Ir}\right) \quad (1)$$

In Equation $E_{T_{(MgXIr_2)}}$ represents the total energy of $MgXIr_2$ (where *X* = Al, Ga, In, and Si) compounds, while E_{Mg}, E_X, and E_{Ir} correspond to the ground state total energies of the Mg, *X*, and Ir atoms, respectively. The negative values ΔE

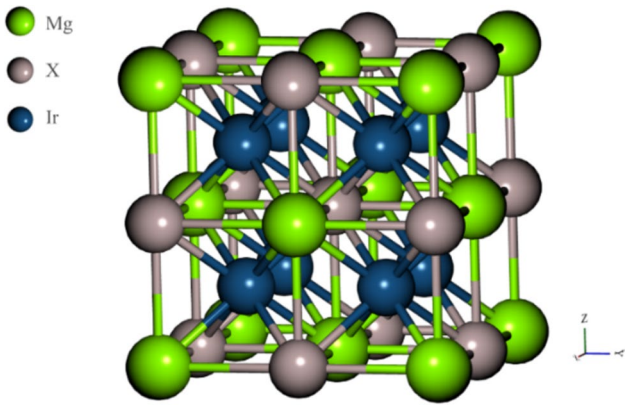

Fig. 1 Crystal structure of full-Heusler MgXIr$_2$ (X = Al, Ga, In, and Si) compounds crystallizing in the cubic L2$_1$ phase with space group $Fm\bar{3}m$. Structural visualization is based on optimized lattice parameters obtained from density functional theory (DFT) total energy minimization.

of the formation enthalpies indicate these compounds as being easily synthesized and thermodynamically stable (Table I).[46] Therefore, these materials are likely to be experimentally synthesizable. Furthermore, the estimated values are in outstanding accord with the existing data.[44, 48]

Elastic constants and related properties

Elastic constants are widely employed to characterize a material's mechanical stability. Corresponding specific heat, thermal expansion, Debye temperature, and Grüneisen parameter as related thermodynamically to elastic properties are decisive for characterizing the mechanical properties of materials because they are associated with essential solid-state phenomena such as interatomic bonding, equations of state, and phonon spectra. The coefficients of proportionality that link applied strain and stress are known as the elastic constants (C_{ij}). As a result, the C_{ij} determine how crystal responds to external influences. While cubic symmetry numbers only contain three elastic constants (C_{11}, C_{12}, and C_{44}), there are 21 independent elastic constants (C_{ij}). Total energy as a function of stress that upsets the volume conservation balance is used to get the elastic constants C_{ij}. The elastic constants of the compounds herein are calculated at their equilibrium lattice constants using the thermo_pw code.

The elastic constants of MgXIr$_2$ alloys, lattice parameter (a_0), bulk modulus (B), shear modulus (G), B/G ratio, formation energy, elastic constants (C_{ij}), were calculated and are presented in Table I. The mechanical parameters, including the shear modulus (G), bulk modulus (B), Young's modulus (E), Poisson's ratio (υ), anisotropy factory (A), Kleinman parameter (ξ) and Cauchy pressure (CP), were estimated using the following equations:

$$G = \frac{C_{11} - C_{12} + 3C_{44}}{5} \tag{2}$$

$$B = \frac{C_{11} + 2C_{12}}{3} \tag{3}$$

$$E = \frac{9BG}{3B + G} \tag{4}$$

$$\nu = \frac{3B - E}{6B} \tag{5}$$

$$CP = C_{12} - C_{44} \tag{6}$$

$$\xi = \frac{C_{11} + 8C_{12}}{7C_{11} + 2C_{12}} \tag{7}$$

The computed elastic constants validate mechanical stability of the alloys by meeting the stability requirements put out by Bhorn[47]: $C_{11} > 0$, $C_{11} + 2C_{12} > 0$, $C_{44} > 0$, and

Table I Lattice parameter (a_0), bulk modulus (B), shear modulus (G), B/G ratio, formation energy, elastic constants (C_{ij}) of MgXIr$_2$ (X = Al, Ga, In, and Si)

Material	Reference	a_0 (Å)	ΔH_f	B (GPa)	G (GPa)	B/G	C_{11}(GPa)	C_{12}(GPa)	C_{44}(GPa)
MgAlIr$_2$	This work	6.111	−0.708	191.119	106.727	1.790	322.199	121.578	112.738
	VASP (GGA) [48]	6.112	−0.702	189	107	1.766	318	124	125
	Theory [44]	6.114	−0.706						
MgGaIr$_2$	This work	6.145	−0.471	190.129	96.778	1.964	303.410	133.489	105.568
	VASP (GGA) [48]	6.114	−0.466	186	96	1.937	293	132	108
	Theory [44]	3.133	−0.463						
MgInIr$_2$	This work	6.373	−0.248	168.107	84.320	1.993	248.013	128.154	105.999
	VASP (GGA) [48]	6.378	−0.259	166	78	2.128	232	132	106
	Theory [44]	6.367	−0.262						
MgSiIr$_2$	This work	6.031	−0.558	216.057	31.112	6.994	223.015	212.579	80.414
	VASP (GGA) [48]	6.037	−0.548	214	88	2.432	340	151	84
	Theory [44]	6.032	−0.600						

C_{11}-$C_{12} > 0$. Bhorn stability criteria indicate that all four compounds are mechanically stable. The calculated elastic constant values C_{ij} presented in Table I for the compounds considered are close to the available theoretical results.[43] The compounds are classified as ductile because the Pugh ratio (B/G)[48] is higher than the crucial threshold (1.75). Furthermore, the calculated positive Cauchy pressure values for GGA ($CP = C_{12} - C_{44}$)[49] show ionic-type bonding and the ductile character of the compounds examined here. The value of Poisson's ratio (υ) implies a strong metallic connection between the component atoms. The estimated mechanical parameters of $MgXIr_2$ compounds such as microhardness parameter, melting point, Kleinman parameter, Young's modulus, Poisson's ratio, and anisotropy factor were calculated, and the findings are shown in Table II.

Young's modulus measures a material's stiffness, and its anisotropy (directional dependence) is crucial for understanding mechanical behavior under stress. $MgIr_2$-based compounds typically exhibit high stiffness due to strong Ir–Ir and Mg–X bonding.

Table II shows that, while $MgAlIr_2$, $MgGaIr_2$, and $MgInIr_2$ exhibit similar properties, $MgSiIr_2$ differs significantly from the others. $MgSiIr_2$ has a very low microhardness (H_v), a very high anisotropy factor (A), a low Young's modulus (E), and a high Poisson ratio (σ). This indicates that the material is softer, more flexible, and more anisotropic (In $MgSiIr_2$, $A = 15.41 \rightarrow$ very high anisotropy, others ~1.1–1.8 → more isotropic). The other three compounds, however, are harder, have higher melting points, and higher Debye temperatures. In $MgSiIr_2$, Kleinman parameter ($\zeta = 0.968$) shows an almost completely ionic bond character, while others ($\zeta = 0.5$–0.6) indicate a covalent–ionic mixed bond structure. $MgAlIr_2$ and $MgGaIr_2$ have a cubic structure and behave almost isotropically. $MgInIr_2$, is cubic but elastically anisotropic. On the other hand, $MgSiIr_2$ has too strong elastic anisotropy to be cubic. Since they all have positive constants, the bond character can be predominantly metallic/ionic and cubic in structure.

In order to quantitatively support the bonding-strength and atomic-size arguments, additional elastic and vibrational parameters were analyzed. As summarized in Table III, the average Ir–X bond length decreases from $MgInIr_2$ to $MgSiIr_2$, with $MgSiIr_2$ exhibiting the shortest bond length (2.6115 Å). Shorter bond lengths are generally associated with stronger interatomic interactions, which directly influence mechanical stiffness.

This trend is further reflected in the phonon characteristics. $MgSiIr_2$ shows systematically higher Γ-point optical phonon frequencies and the highest maximum phonon frequency among the investigated compounds, indicating stiffer bonds and higher vibrational energy scales. Although Γ-point frequencies alone do not determine the Debye temperature, their relative upward shift provides a clear indication of enhanced bond stiffness. Together with the elastic constants reported in Tables I and II, these results quantitatively explain the observed variations in Young's modulus and Debye temperature across the $MgXIr_2$ series.

Substitution of X (Al, Ga, In, and Si) influences bonding strength and thus Si shows higher E because of its smaller atomic radius, and stronger covalent bonding character than others (Fig. 2). Covalent bonding (Si) enhances E, while

Table II The microhardness parameter (H_v), melting point (T_m), Kleinman parameter (ζ), Young modulus (E), Poisson's ratio (σ), anisotropy factor (A), Debye temperature (θ_D) of $MgXIr_2$ (X = Al, Ga, In, and Si) compounds

Material	Reference	H_v	T_m (K)	ζ	CP (C_{12}-C_{44}) (GPa)	E (GPa)	σ	A	θ_D (T)
$MgAlIr_2$	This work	17.138	1219.281	0.518	8.840	269.935	0.26	1.123	396.096
	VASP (GGA) [43]	–	–	–	8.840	270.17	0.26		–
$MgGaIr_2$	This work	14.220	1176.906	0.573	27.921	248.218	0.28	1.242	361.375
	VASP (GGA) [43]	–	–	–	24	246.54	0.28		–
$MgInIr_2$	This work	12.414	1179.454	0.639	22.155	216.687	0.28	1.768	326.886
	VASP (GGA) [43]	–	–	–	22.155	204.19	0.29		–
$MgSiIr_2$	This work	2.0850	1028.246	0.968	132.165	87.574	0.40	15.410	194.597
	VASP (GGA) [43]	–	–	–	67	253.77	0.32		–

Table III Γ-point optical phonon frequencies and maximum phonon frequencies

Materials	$\omega_1(\Gamma)$	$\omega_2(\Gamma)$	$\omega_3(\Gamma)$	$\omega_{av}(\Gamma)$	$\omega_{max}(X)$	$\langle d \rangle$ Ir–X (Å)
$MgAlIr_2$	4.407787	8.553803	10.639156	7.866915	11.443253	2.64614
$MgGaIr_2$	4.077837	5.737542	10.052032	6.622470	10.397160	2.66086
$MgInIr_2$	3.691593	5.586553	8.6768280	5.984991	9.0812580	2.75959
$MgSiIr_2$	4.475878	6.796061	11.033702	7.435214	12.523626	2.61150

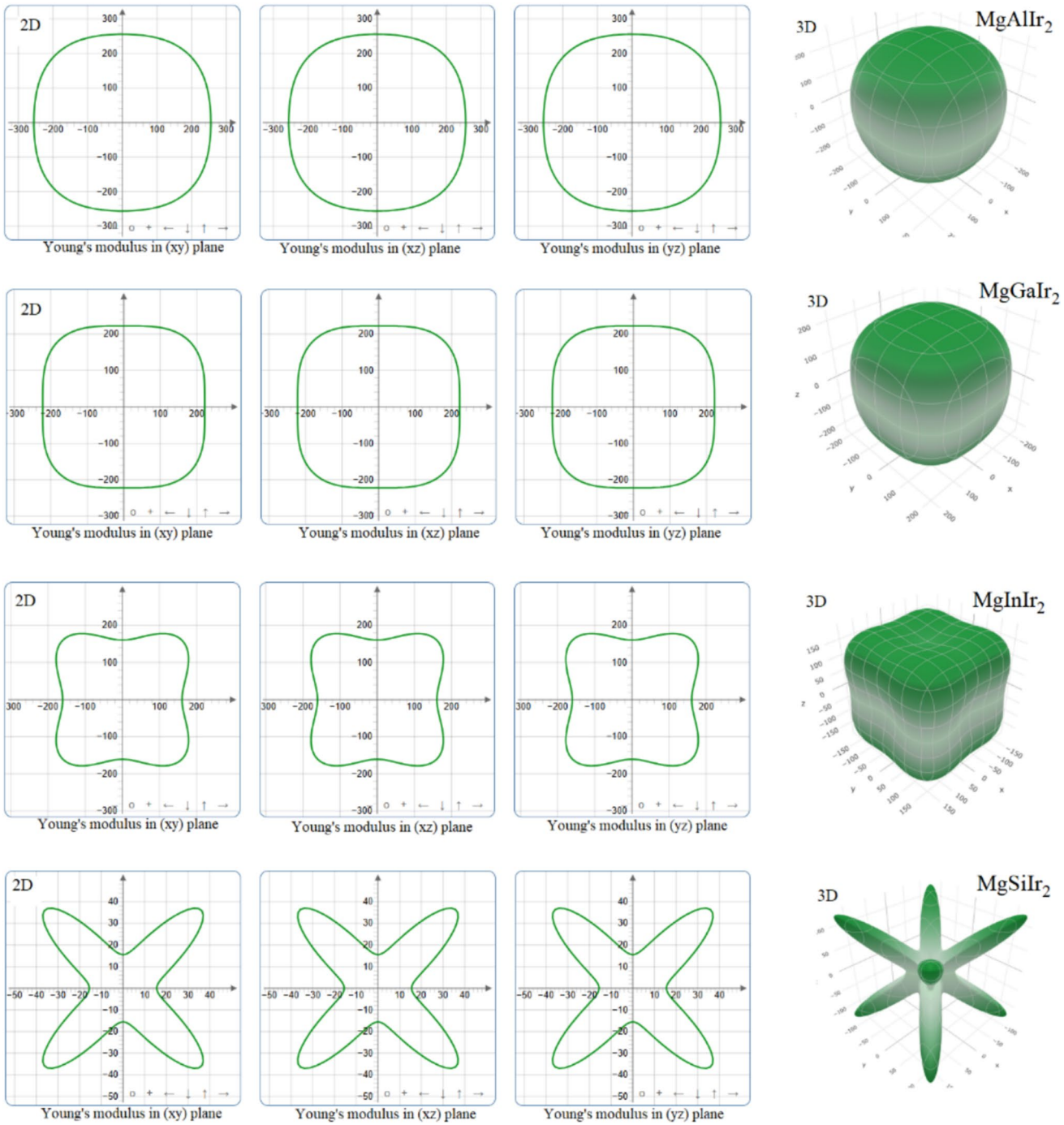

Fig. 2 Two-dimensional and three-dimensional representations of the directional Young's modulus for $MgXIr_2$ (X = Al, Ga, In, and Si) compounds, calculated from the full elastic tensor using the Voigt–Reuss–Hill averaging scheme. The elastic constants were obtained via the energy–strain method as implemented in the thermo_pw package.

metallic bonding (In) reduces it. All of them have cubic structures and near-isotropic E (similar in all directions).

Young's Modulus surfaces in 3D provide a spatial representation of stiffness. No VRH polycrystalline averages are used on these surfaces. The lobes align with cubic directions $<100>$, $<110>$, $<111>$. $MgSiIr_2$ exhibits stronger lobes along $<111>$, consistent with its shorter Ir–Si bond length and enhanced covalent hybridization. Therefore, $MgSiIr_2$ (i-doped) shows the highest E due to strong Si–Ir covalent contributions. $MgInIr_2$ (In-doped) may have the lowest E due to metallic bonding softening.

$MgAlIr_2$ and $MgGaIr_2$ should lie in between, with Ga slightly stiffer than Al due to shorter bond lengths.

Figure 3 shows the calculated electronic band profiles of $MgXIr_2$ (X = Al, Ga, In, and Si) compounds in full Heusler phase along the high symmetry direction in BZ. A dashed line indicates that the Fermi level (E_F) is set to zero. The electronic band profiles of the four compounds shown in Fig. 3 are very similar. All band structures were computed along the standard FCC path Γ–K–X–Γ–L–X–M–L corresponding to the Fm-3 m structure. Spin-orbit coupling (SOC) tests showed small shifts (0.05–0.15 eV) in Ir-5*d* states but no modification of metallicity. All compounds converge to nonmagnetic ground states, so no spin splitting occurs.

The overlapping values of the electronic states at the Fermi level are evidence that the investigated compound exhibits metallic conductivity. As evidenced by the electronic band profiles in Fig. 3, the conduction band minima and valence band maxima exhibit an overlap at the Fermi level, confirming the metallic character of the investigated compounds.

To further analyze the electronic band profile of $MgXIr_2$ (X = Al, Ga, In, and Si) compounds, we examine the total density of states (TDOS) and the partial density of states (PDOS), as presented in Fig. 4. As is clearly seen as a reflection of the electronic band profile, states with overlap at the Fermi level are observed, indicating the metallic behavior of these materials. As can be seen from the PDOS (in Fig. 4), near the Fermi level, the Ir-5*d* states contribute more to the metallic nature of the materials, with less contribution from other electronic states. For all four compounds studied herein, a large peak starting near the Fermi energy level and extending to around −6 eV is due to the contribution of Ir-5*d* states. The sum of PDOS reproduces TDOS within < 1% error. Ir-5*d* states dominate the −2 to + 1 eV region. $MgGaIr_2$ and $MgInIr_2$ show mild van Hove-like features just below EF, but phonon spectra confirm dynamical stability. Furthermore, the contribution of Ir-5*d* states is evident in a small peak just above the Fermi level, within the 0–2 eV range. $MgXIr_2$ compounds are metallic in nature, so the density of states at the Fermi level, a parameter known as $N(E_F)$, is a critical parameter for electronic stability. The

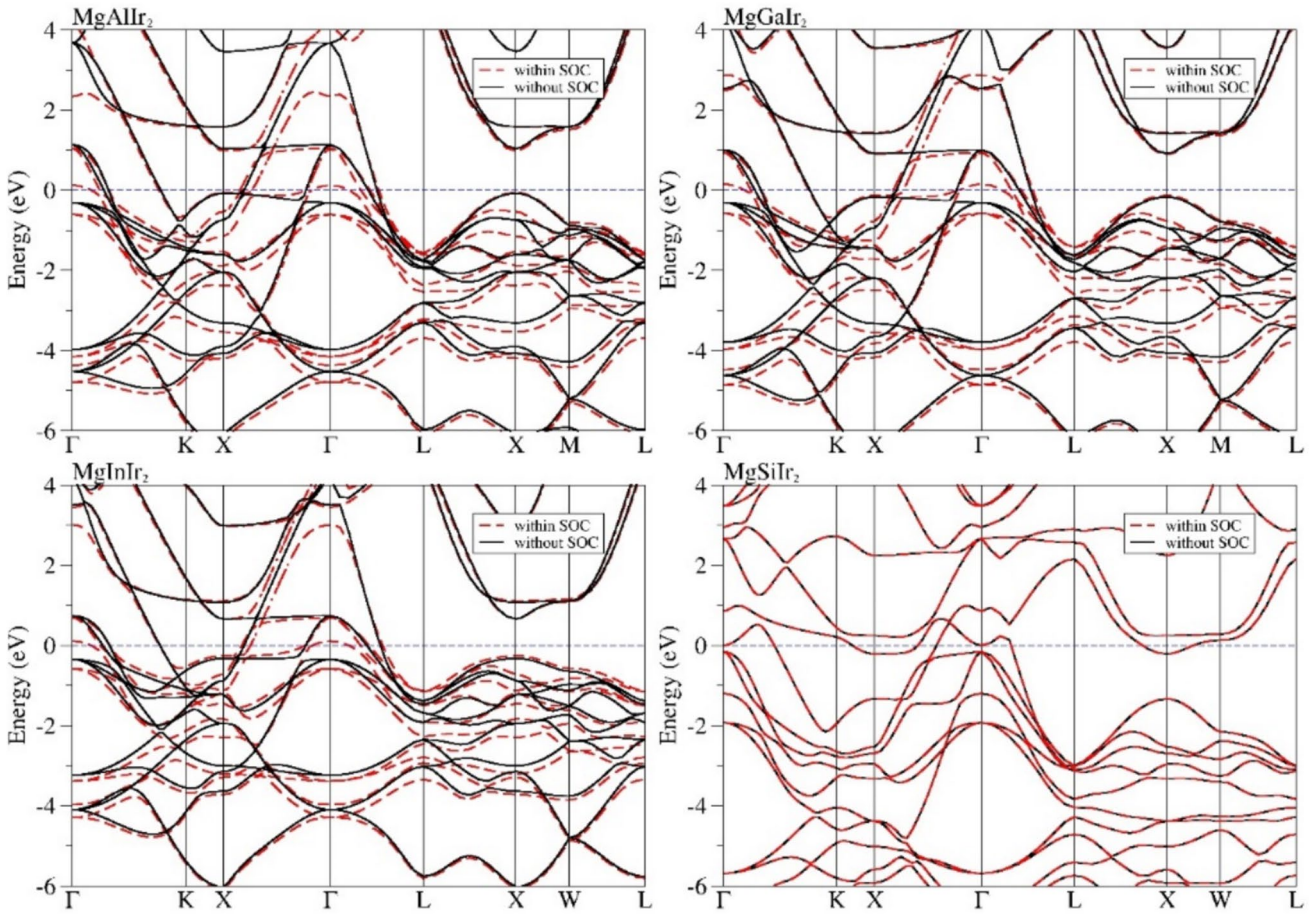

Fig. 3 Electronic band structures of full-Heusler $MgXIr_2$ (X = Al, Ga, In, and Si) compounds calculated along high-symmetry directions in the Brillouin zone using DFT within the GGA-PBE approximation. The Fermi level is set to zero energy.

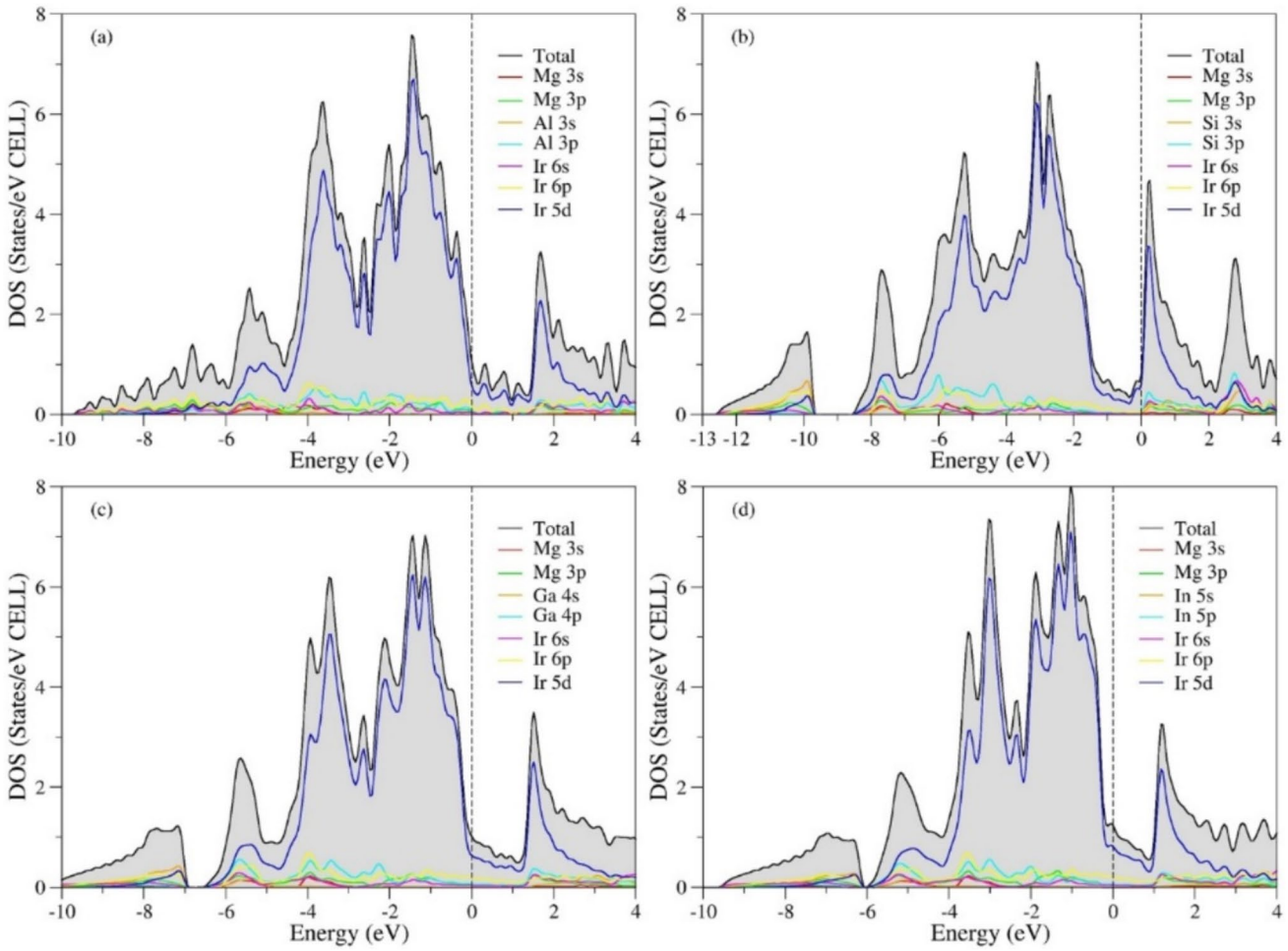

Fig. 4 Total and projected electronic density of states (TDOS and PDOS) of $MgXIr_2$ (X = Al, Ga, In, and Si) compounds calculated using DFT-GGA. Contributions from individual atomic orbitals highlight the dominant role of Ir-5*d* states near the Fermi level.

location of the Fermi level and the value of $N(E_F)$ contribute to the phase stability of intermetallic compounds. A system with a smaller $N(E_F)$ is more stable than one with a larger $N(E_F)$. The value of the Fermi level $N(E_F)$ of $MgAlIr_2$, $MgGaIr_2$, $MgInIr_2$, and $MgSiIr_2$ compounds are 2.065 states/eV, 2.118 states/eV, 2.580 states/eV, and 1.550 states/eV CELL, respectively. On the basis of these estimated values, electronically more stable materials are classified as $MgSiIr_2 > MgAlIr_2 > MgGaIr_2 > MgInIr_2$. Thus, $MgSiIr_2$ is electronically more stable than the other compounds.

Phonons are essential for the study of new materials such as dynamic behavior and thermal conductivity. Positive and negative phonon modes provide insights into the dynamic stability or instability of a material using phonon dispersion curves. Negative frequency modes indicate dynamic instability in a compound, while positive phonon frequency modes indicate dynamic stability in a material. Phonon paths follow the cubic FCC sequence Γ–K–X–Γ–L–X–M–L. Calculations used a 4×4×4 q-mesh. Displacement amplitude was 0.01 Å. Nonanalytical term corrections (Born charges) were not applied, as all the compounds are metallic and LO–TO splitting is not defined for metals.

Figure 5 depicts the phonon density of states of four Heusler compounds, including total DOS and partial DOS (PDOS), as well as the phonon spectra along high-symmetry directions in the Brillouin zone. The phonon dispersion curves of the studied four compounds has similar shapes. The investigated materials' primitive unit cells comprise four atoms, resulting in a total of 12 vibrational modes: three acoustic modes and nine optical modes. The lack of negative frequencies in the entire phonon spectra and density of states (total and partial DOS) of $MgXIr_2$ (X = Al, Ga, In, and Si) compounds indicates that they are dynamically stable, as seen in Fig. 5. For the four examined materials, the full phonon spectra contain bandgaps starting approximate 3. 4 THz. This property of the compounds may result in their employment in a variety of applications, including sound filters, mirrors, and phonon bandgaps. Sound is simply reflected

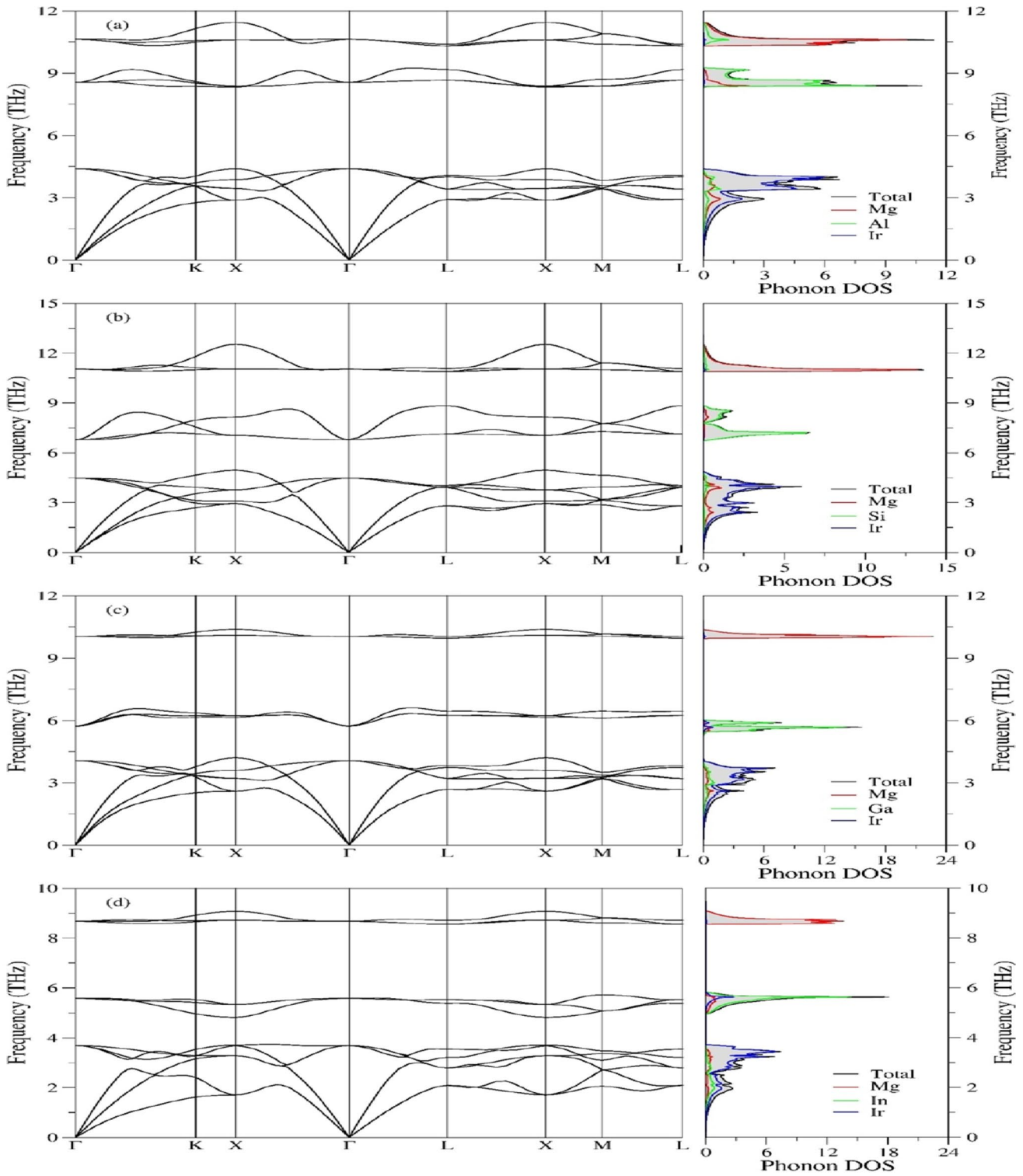

Fig. 5 Phonon dispersion relations of $MgXIr_2$ (X = Al, Ga, In, and Si) compounds calculated using density functional perturbation theory (DFPT). The dynamical matrices were computed on a 4×4×4 **q**-point mesh and interpolated along high-symmetry directions in the Brillouin zone. Spin–orbit coupling was not included in the phonon calculations, and no nonanalytical corrections were applied. The absence of imaginary frequencies confirms the dynamical stability of all compounds.

from the surface and does not go across the gap.[50, 51] For the compounds studied here, the lowest optical modes and acoustic modes overlap with each other below approximate 3.4 THz.

To examine the full phonon dispersion curves in more detail, the corresponding partial and total phonon density of states (DOS) is shown in Fig. 5. Species-resolved PDOS correctly reproduce total DOS. The q-mesh was $4\times4\times4$ with Gaussian broadening of 0.15 THz. Sharp peaks were smoothed by increasing broadening. Frequencies follow mass hierarchy: Ir (3–4 THz), Mg (5–7 THz), and X atoms shifting with mass (Si > Al > Ga > In). No artificial localization was observed. The heavier Ir atoms contribute to lattice vibrations in the low frequency areas (3.4 THz). For the investigated $MgXIr_2$ (X = Al, Ga, In, and Si) compounds, the upper two optical phonon modes also exhibit distinct separation. The results from Fig. 5 confirm that Mg atoms contribute to the formation of phonon vibrations in the frequency range of $MgAlIr_2$ at around 9 THz, $MgGaIr_2$, $MgInIr_2$, and $MgSiIr_2$ at about 6 THz. The highest frequency range of $MgXIr_2$ (X = Al, Ga, In, and Si) compounds exhibit the contribution of X atoms.

In this study, we studied the temperature dependence of various thermodynamic properties of $MgXIr_2$ full-Heusler compounds in the range of 0–800 K using whit Quasi-harmonic approximations (QHA) implemented in the Thermo_PW package. Thermodynamic properties such as free energy, enthalpy, entropy, and constant volume heat capacity in both volumes are vital for controlling material stability. The estimated temperature dependence of free energy and enthalpy (Energy) is depicted in Fig. 6a and b. As illustrated in Fig. 6b, free energy decreases progressively with increasing temperature and eventually approaches zero, subsequently attaining negative values. In contrast, enthalpy exhibits a continuous increase as the temperature rises. In addition, the calculated entropy shows a noticeable increase with increasing temperature, suggesting that higher thermal energy leads to more pronounced oscillations of the crystal planes (Fig. 6c). Heat capacity analysis yields complementary information—revealing details of the

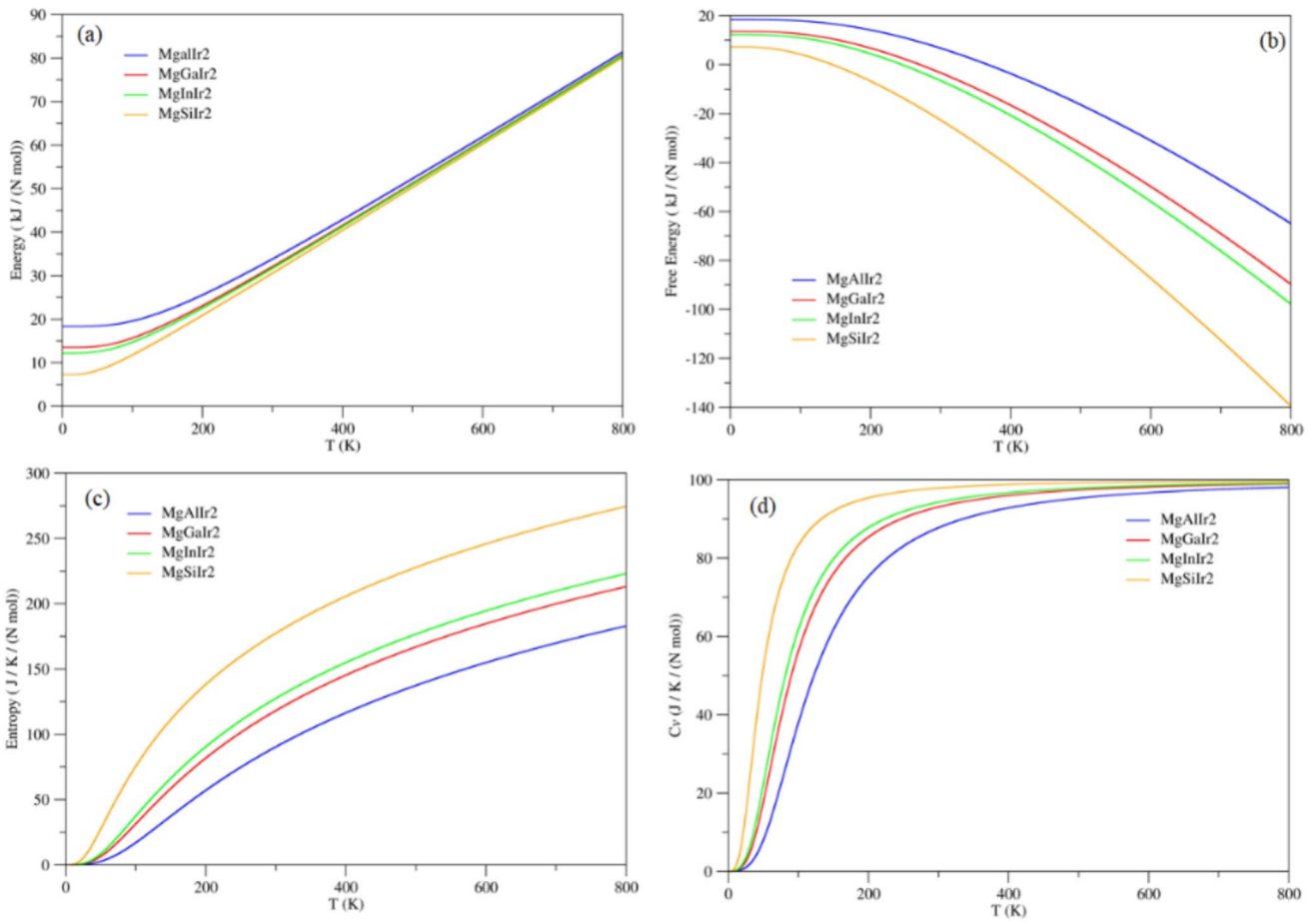

Fig. 6 Total and partial phonon density of states (DOS) of $MgXIr_2$ (X = Al, Ga, In, and Si) compounds obtained from DFPT calculations using a $4\times4\times4$ **q**-point mesh. The phonon DOS was constructed via Fourier interpolation of the interatomic force constants. Contributions from Mg, Ir, and X atoms are shown to elucidate the atomic origin of vibrational modes.

vibrational density of states while constraining the material's operational temperature range for applications. The constant-volume specific heat capacity of $MgXIr_2$ is displayed in Fig. 6d. Heat capacity reaches the limit in $MgSiIr_2$ earlier than in $MgAlIr_2$, showing enhanced thermal stability up to higher temperatures, greater density of states near the Fermi level, and superior high-temperature performance for potential applications.

Conclusions

Mg-based alloys have emerged as a critically important class within every material in recent years. Their inherent biodegradability in physiological environments renders them highly suitable for the fabrication of temporary orthopedic implants. $MgSiIr_2$ are high-E materials, useful in high-stress applications with high E, while lower E materials such as $MgInIr_2$ need better ductility and toughness.

The design of novel Mg-based alloys for medical tenders requires careful selection of alloying elements, with particular emphasis on their systemic toxicity profiles, as these elements play a crucial role in enhancing mechanical properties and corrosion resistance by modifying the compound microstructure. Furthermore, metallurgical considerations, particularly the interplay between chemical composition, processing techniques, and resultant properties—must be thoroughly evaluated, as these factors significantly influence the functional performance of the final material.

Future research should prioritize the development of compounds exhibiting a controlled degradation rate and superior mechanical endurance to address load-bearing applications. In addition, exploring new biocompatible alloying elements remains essential. Advancements in orthopedic implant design, particularly for foot and ankle surgery, will depend on a stronger correlation between clinical requirements and the biofunctional properties of Mg-based alloys. Currently, no universally optimal Mg-based alloy exists for all orthopedic applications, underscoring the necessity for further research, including clinical trials, to validate each newly developed implant.

Beyond these directions, we anticipate a change in basic assumptions in the application of Mg-based alloys—from small implants to larger bone defect repairs or hybrid systems combining biodegradable metals, ceramics, and polymers.

Funding Open access funding provided by the Scientific and Technological Research Council of Türkiye (TÜBİTAK).

Conflict of interest The authors declare that they have no known competing financial interests or personal relationships that could have appeared to influence the work reported in this paper.

References

1. V. Abdul Shukoor, M. Sarwan, and S. Singh, High pressure structural, elastic and electronic properties of a new half Heusler compound: AuYPb. *Phys. B* 547, 83–87 (2018).
2. M. Sarwan, A. Gour, V. Abdul Shukoor, S. Singh, 2019 High pressure study of half Huesler alloy: YPdSb. in AIP Conference Proceedings. 2100, No. 020158.
3. T. Zhu, C. Fu, H. Xie, Y. Liu, and X. Zhao, High efficiency half-Heusler thermoelectric materials for energy harvesting. *Adv. Energy Mater.* 5, 1500588 (2015).
4. L. Huang, Q. Zhang, B. Yuan, X. Lai, X. Yan, and Z. Ren, Recent progress in half-Heusler thermoelectric materials. *Mater. Res. Bull.* 76, 107–112 (2016).
5. C. Felser, L. Wollmann, S. Chadov, G.H. Fecher, and S.S.P. Parkin, Basics and prospective of magnetic Heusler compounds. *APL Mater* 3, 041518 (2015).
6. T. Kojima, S. Kameoka, and A.P. Tsai, Correction to: Heusler alloys: a group of novel catalysts. *ACS Omega* 3, 9738 (2018).
7. T. Kojima, S. Kameoka, and A.P. Tsai, Catalytic properties of Heusler alloys for steam reforming of methanol. *ACS Omega* 4, 21666–21674 (2019).
8. C. Kim, W. Yoo, H.W. Bang, S. Lee, Y.C. Park, Y.H. Lee, J. Choi, Y. Jo, K. Lee, and M.H. Jung, Highly reduced saturation magnetization in epitaxially grown ferrimagnetic Heusler thin films. *ACS Omega* 4, 16578–16584 (2019).
9. B. Govind, A. Kumar, S. Bano, A. Bhardwaj, and D.K. Misra, Structural and magnetic properties of Ni1+ XMnSb bulk Heusler composite materials. *ACS Omega* 5, 11895–11900 (2020).
10. S.Y. Lin, M. Chen, X.B. Yang, Y.J. Zhao, S.C. Wu, C. Felser, and B. Yan, Theoretical search for half-Heusler topological insulators. *Phys. Rev* 91, 094107 (2015).
11. J.W.G. Bos, and R.A. Downie, Half-Heusler thermoelectrics: a complex class of materials. *J Phys: Condens Matter.* 26, 433201 (2014).
12. M. Asif, A.O. Alrashdi, M.M. Fadhali, A. Afaq, and A. Bakar, First-principles investigations of thermoelectric behavior of RuCrX (X = Si,Ge, Sn). *ACS Omega* 7, 45353–45360 (2022).
13. X. Chen, X. Zhang, J. Gao, Q. Li, Z. Shao, H. Lin, and M. Pan, Computational search for better thermoelectric performance in nickel-based half-Heusler compounds. *ACS Omega* 6, 18269–18280 (2021).
14. S. Tavares, K. Yang, and M.A. Meyers, Heusler alloys: past, properties, new alloys, and prospects. *Prog. Mater. Sci* 132, 101017 (2023).
15. W. Everhart, and J. Newkirk, *Mechanical properties of Heusler alloys. Heliyon.* 5, e01578 (2019).
16. Z.P. Hao, R. Liu, Y.H. Fan, and L.L., Wang, First-principles calculations of a new half-metallic Heusler alloy FeCrAs. *J. Alloys Compd.* 820, 153118 (2020).

17. X.P. Wei, Y.D. Chu, X.W. Sun, J.B. Deng, and Y.Z. Xing, Stability, electronic, magnetic and pressure effect of half-Heusler alloys CNaCa and SiNaCa: a first-principles study. *Superlattices Microstruct.* 74, 70–77 (2014).
18. N. Arikan, S. Al, and A. Iyigör, Mechanical, electronic, thermodynamic and vibrational properties of X_2MgAl (*X*= Sc, Ti and Y) from first principles calculations. *J. Mol. Model.* 28(11), 366 (2022).
19. I. Antoniac, M. Miculescu, V. Mănescu, A. Stere, P.H. Quan, G. Păltânea, A. Robu, and K. Earar, Magnesium-based alloys used in orthopedic surgery. *Materials* 15(3), 1148 (2022).
20. R. Paudel, K.C. Santosh, S. Adhikari, J. Zhu, S. Ahmad, G.C. Kaphle, and D. Paudyal, Electronic and magnetic properties of iridium-based novel Heusler alloys. *J. Magn Magn Mat.* 555, 169405 (2022).
21. M. Çanlı, E. Ilhan, and N. Arıkan, First-principles calculations to investigate the structural, electronic, elastic, vibrational and thermodynamic properties of the full-Heusler alloys X_2ScGa (*X*= Ir and Rh). *Mater Today Comm.* 26, 101855 (2021).
22. M.A.U. Islam, M.R. Islam, O. Das, S. Kato, N. Kishi, and T. Soga, First-principles calculations to investigate the stability and thermodynamic properties of a newly exposed lithium–gallium–iridium-based full-heusler compound. *ACS Omega* 8(24), 21885–21897 (2023).
23. C. Kanagaraj, M. Prakash, and M. Navaneethan, Unveiling the half-metallic features of IrMnCrZ (*Z*= Al, Ga, In, Si, Ge, Sn, P, As and Sb) alloys for spintronic applications. *Phys. Scr.* 100(5), 055517 (2025).
24. E.M. Mozur, and R. Seshadri, Magnetic tunability in tetragonal Mn–Rh–Ir–Sn inverse Heusler compounds. *J. Condens. Matter Phys.* 36(19), 195802 (2024).
25. H. Masumoto, K. Watanabe, and S. Ohnuma, New compounds of the Cl_b, Cl types of IrMnSb and PdMnTe, New $L2_1$(Heusler) type of Ir_2MnGa alloys, and magnetic properties. *J. Phys. Soc. Japan* 32, 570 (1972).
26. S. Krishnaveni, Halfmetallicity, mechanical and thermodynamic study on iridium-based compounds by first principles calculations. *Mater. Res. Express* 6(9), 096545 (2019).
27. S. Krishnaveni, 2019 Electronic band structure analysis on newly proposed iridium-based Heusler alloys in different exchange correlation potentials, J. Phys. Conf. Ser. 1172 012041 (1)
28. K. Balakrishnan, S. Alagarsamy, and V. Veerapandy, First-principles investigation on thermoelectric and vibrational properties of half-metallic Ir_2MnX (*X*= B, Al, Ga, In) Heusler alloys. *Phys. status solidi (b)* 260(1), 2200329 (2023).
29. A. Candan, A study on magnetic, electronic, elastic and vibrational properties of Ir_2MnAl Heusler alloy for spintronic applications. *Mater. Res. Express* 6(9), 096571 (2019).
30. G. Forozani, F. Karami, and M. Moradi, Structural, electronic, magnetic and vibrational properties of full-Heusler Ir_2CrX (X = Si, Ge) compounds. *Acta Phys. Pol. A* 137, 430 (2020).
31. G. Forozani, F. Karami, and M. Moradi, Structural, electronic, magnetic, and optical properties of Ir_2ScZ (Z = Si, Ge, Sn) full-Heusler compounds: a first-principles study. *J. Electron. Mater.* 49(10), 5947–5956 (2020).
32. E.G. Özdemir, E. Eser, and Z. Merdan, Investigation of structural, half-metallic and elastic properties of a new full-Heusler compound–Ir_2MnSi. *Chin. J. Phys.* 56(4), 1551–1558 (2018).
33. S.L. Gupta, S. Kumar, S.S. Anupam, S. Thakur, and D. Diwaker. Panwar, A newly proposed full Heusler alloy Ir_2V Z (*Z*= Sn, In) suitable for high-temperature thermoelectric applications: a DFT approach. *Mod Phys Lett B.* 38(09), 2450030 (2024).
34. R. Prakash, and G. Kalpana, Prediction of structural, electronic and magnetic properties of full Heusler alloys Ir_2YSi (Y = Sc, Ti, V, Cr, Mn, Fe Co, and Ni) via first-principles calculation. *AIP Adv.* 11(1), 015042 (2021).
35. A. Iyigör, S. Al, and N. Arikan, Density functional theory investigation on structural, mechanical, electronic and vibrational properties of Heusler alloys $AlXIr_2$ (*X*= Co, Cr, Cu, Fe and Zn). *Chem. Phys. Lett.* 806, 140052 (2022).
36. N. Arikan, H.Y. Ocak, G. Dikici Yıldız, Y.G. Yıldız, and R. Ünal, Investigation of the mechanical, electronic and phonon properties of X_2ScAl (*X*= Ir, Os, and Pt) Heusler compounds. *J. Korean Phys. Soc.* 76(10), 916–922 (2020).
37. N.T. Hung, A.R. Nugraha, R. Saito, Quantum ESPRESSO course for solid-state physics. (Jenny Stanford Publishing, 2022).
38. J.P. Perdew, K. Burke, and M. Ernzerhof, Generalized gradient approximation made simple. *Phys. Rev. Lett.* 77, 3865–3868 (1996).
39. M. Ma, G. Liu, X. Gao, and G. Zhang, First-principles study of the effect of S-atom doping on the optoelectronic properties of stanene. *J. Mol. Model.* 30(4), 115 (2024).
40. N. Rivano, N. Marzari, and T. Sohier, Density functional perturbation theory for one-dimensional systems: Implementation and relevance for phonons and electron-phonon interactions. *Phys. Rev. B* 109(24), 245426 (2024).
41. H. Li, Z. Tang, J. Fu, W.H. Dong, N. Zou, X. Gong, W. Duan, and Y. Xu, Deep-learning density functional perturbation theory. *Phys. Rev. Lett.* 132(9), 096401 (2024).
42. R. Gaillac, P. Pullumbi, and F.X. Coudert, ELATE: an open-source online application for analysis and visualization of elastic tensors. *J. Condens. Matter Phys.* 28(27), 275201 (2016).
43. K. Latimer, S. Dwaraknath, K. Mathew, D. Winston, K.A. Persson, 2018 Evaluation of thermodynamic equations of state across chemistry and structure in the materials project. npj Comput Mater. 4 1 40
44. J.E. Saal, S. Kirklin, M. Aykol, B. Meredig, and C. Wolverton, Materials design and discovery with high-throughput density functional theory: the open quantum materials database (OQMD). *Jom* 65, 1501–1509 (2013).
45. Y. Pan, and S. Chen, Exploring the novel structure, transportable capacity and thermodynamic properties of TiH_2 hydrogen storage material. *Int. J. Energy Res.* 44(6), 4997–5007 (2020).
46. N. Xu, Y. Chen, S. Chen, S. Li, and W. Zhang, First-principles investigation for the hydrogen storage properties of $XTiH_3$ (^{X}= K, Rb, Cs) perovskite type hydrides. *Int. J. Hydrogen Energy* 50, 114–122 (2024).
47. M. Born, On the stability of crystal lattices. I. In Mathematical Proceedings of the Cambridge Philosophical Society (Vol. 36, No. 2, pp. 160-172) (Cambridge University Press, 1940).
48. S.F. Pugh, and XCII., Relations between the elastic moduli and the plastic properties of polycrystalline pure metals. *Lond Edinb Dubl Phil Mag* 45(367), 823–843 (1954).
49. S.J. Zaidi, M.I. Khan, S.S.A. Gillani, M.S.U. Sahar, S. Ullah, and M. Tanveer, A comprehensive DFT study to evaluate the modulation in the band gap, elastic, and optical behaviour of $CsPbBr_3$ under the effect of stress. *Mater. Res. Express* 9(12), 125501 (2022).
50. J. Kangsabanik, M.K. Svendsen, A. Taghizadeh, A. Crovetto, and K.S. Thygesen, Indirect band gap semiconductors for thin-film photovoltaics: high-throughput calculation of phonon-assisted absorption. *J. Am. Chem. Soc.* 144(43), 19872–19883 (2022).
51. N. Arıkan, O. Örnek, A. İyigör, and M. Çanlı, Investigation on the structural, elastic, electronic, thermodynamic, and vibrational properties of the full Heusler Sc_2XAl (*X*= Cd and Zn): an *ab initio* study. *Physica B* 695, 416492 (2024).